IEEE Access
Multidisciplinary | Rapid Review | Open Access Journal

Received November 8, 2019, accepted December 9, 2019, date of publication December 16, 2019,
date of current version December 23, 2019.

Digital Object Identifier 10.1109/ACCESS.2019.2959800

Patch-Wise Blind Image Deblurring via Michelson Channel Prior

GUOQUAN WEN[1,2], CHAO MIN[1,2], (Member, IEEE), ZEYUN JIANG[3], ZHAOZHONG YANG[4], AND XIAOGANG LI[4]

[1]School of Science, Southwest Petroleum University, Chengdu 610500, China
[2]Institute of Artificial Intelligence, Southwest Petroleum University, Chengdu 610500, China
[3]Institute of Petroleum Engineering, Heriot-Watt University, Edinburgh EH14 4AS, U.K.
[4]State Key Laboratory of Oil and Gas Reservoir Geology and Exploitation, Southwest Petroleum University, Chengdu 610500, China

Corresponding author: Chao Min (minchao@swpu.edu.cn)

This work was supported in part by the National Natural Science Foundation of China under Grant 11601451 and Grant 11526173.

ABSTRACT Motion blur exists in many computer vision tasks, including faces, texts, and low-illumination images etc. It has been proved that Dark Channel Prior (DCP) and Bright Channel Prior (BCP) can both help the image deblurring by enhancing the dark or bright channel pixels. However, the pixels between the dark channel pixels and the bright channel pixels are not taken into consideration, which limits the deblurring performance. A novel image channel is proposed in combination with dark channel and bright channel in this paper to consider the effects of the all types of pixels, namely, Michelson channel pixels. Secondly, as the image channels are built based on the series of image patches with different blur kernels, a new method is developed to estimate the blur kernel and can measure the similarity between neighbored kernels. Meanwhile, to perform accurate kernel estimation, the L_0 regularization is applied into the algorithm framework. In the process of image deblurring, by enhancing the Michelson channels and retaining the other channels of the image, we can capture sharper image detail and eliminate the ringing artifacts of the recovered images. Massive experimental results demonstrate that the proposed method is more robust and outperforms the existing art-of-the-state of unsupervised image deblurring methods on both synthesized and natural images.

INDEX TERMS Blind image deblurring, Michelson channel prior, L_0 gradient minimization.

I. INTRODUCTION

In computer vision, the problem regarding to the image restoration including super-resolution, blur and noise removal is a classical vision problem, which has obtained significant progress in recent years [1]–[6]. The goal of blurs removal, e.g., image deblurring, is to effectively estimate the blur kernel and latent image from the blurred image. With the assumption that the blur is spatially invariant, the image blur process can be modeled as:

$$B = L * K + N \tag{1}$$

where B, L, K, and N denote the blurred image, latent image, blur kernel, and noise, respectively; and $*$ is the convolution operator.

Blind image deblurring is an ill-posed problem [7], [8], which contains the infinite pairs of L and K and can give rise to the corresponding B refer to the equation (1). Therefore, various deblurring methods are proposed by utilizing the additional information of L, K and B to control the solution space in image deblurring. Then multiple deblurring methods recover the degraded image [9]–[11] via constraining the solution space of blurred images. For example, numerous methods [12]–[14] utilize the gradient sparsity prior or total variation to recover the blurred images. Meanwhile, many scholars presented some new image priors to recover the clean images over blurred images, e.g., L_0-regularized prior [14] and low-rank prior [15]. Levin *et al.* [16] show that suitable gradients of blurred image can help improve blur kernel and latent image estimation by using statistical fitting. In addition, some existing deblurring methods focus on detecting sharp edge of under-truly image on the process of image restoration [14], [17].

Dark channel is firstly proposed by the He *et al.* [18] for the color image dehazing, which can be modeled as follows.

$$\begin{aligned} D(I)(x) &= \min_{y\in\Omega(x)}\left(\min_{c\in\{r,g,b\}} I^c(y)\right) \\ &= \min_{y\in\Omega(x)}\left(\min_{c\in\{r,g,b\}} t(x)J^c(x) + (1-t(x))\mathbf{A}\right) \end{aligned} \tag{2}$$

The associate editor coordinating the review of this manuscript and approving it for publication was Naveed Akhtar.

where D(·) denotes the dark channel operator; I is the haze image; J is the haze-free image; A denotes the atmospheric light component; and t denotes the transmittance; x denotes the pixels of image including clear image and degraded image; y denotes the pixels of patch image $\Omega(x)$ ($\Omega(x)$ is an image patch centered at x); and I^c and J^c represent the c-th color channel of clear image and haze image, respectively.

In [19], Jinshan Pan et al. observe that enforcing the sparsity of the dark channel can help blind deblurring on various scenarios, including face, text and low-illumination images in the process of kernel and latent image estimation. Subsequently, Yan *et al.* [20] observed that the bright pixels are also dominated the clear images. Therefore, the bright channel prior is proposed to image deblurring. We have studied the theory and effect of the dark channel prior and bright channel prior in the image deblurring. What can be confirmed is that the sufficient dark pixels and bright pixels of the image can significantly affect the deblurring performances, which is similar to massive methods of image dehazing, like the work [21], [22]. In [22], Kim J H et al. restore the hazy image by minimizing the cost function which consists of the contrast term and the information loss. In [21], Schaul L et al. propose a method by using a near-infrared (NIR) image to dehaze the color image. And we observe that the work [18], [21], [22] are essentially designed to capture one of channel pixels of degraded images for image restoration.

Based on the above observation, a new blind image deblurring method is presented in this paper, which is aiming at capturing Michelson channel pixels when highlighting dark channel pixels and bright channel pixels. Meanwhile, we proposed a new metric method for more accurate estimation of blur kernels. With the proposed method, we can effectively remove the ringing artifacts and estimate the latent image. The detail of mathematical modelling process is given in Section III of this paper. The core contributions are summarized as follows,

1) A novel image channel, Michelson channel, is proposed to capture the details of the latent image over the blurred image and to restore the blurred image.
2) The values of Michelson channel pixels are mathematically proved to decrease after the blurring process of the clean image. And the effectiveness of the proposed method is validated by comparing the intensities of Michelson channel pixels on the clear images and the corresponding blurred image and comparing the deblurring performance of the other classical methods.
3) A new metric method is defined to measure the similarity between the blur kernels of the corresponding image patches. According to the metric value, we can adjust the influence of different image patches on the estimated latent image by the corresponding weight parameters, and then obtain the optimal solution.

II. RELATED WORK

In recent years, computer vision obtains significant progress along with the rise of image prior and deep learning [[4], [14], [16], [19], [23], [6] etc.]. For a single image blur removal, it also has obtained the significant progress [[2], [24], [25], [26] etc.]. Based on statistical prior and sharp edge characteristics of images, massive methods have been proposed to estimate the clear image and blur kernel [[7], [12], [14], [19] etc.].

To estimate blur kernels from blurred images, the statistical priors [15] is applied to solve the ill-posed problem [8]. Based on the hyper-Laplacian prior, Levin *et al.* [16] proposed a maximum a posterior (MAP) framework to estimate the latent image. Xu *et al.* [9], [27], [28] have proven that the two-phase kernel estimation is helpful for the image deblurring. In [10], Pan et al. propose a kernel estimation model to preserve the sparsity and continuity of blur kernels, then to preserve the edge features of latent image. Joshi *et al.* [17] present a blur kernel estimation algorithm by using the sharp edge of the subpixel resolution from a single image. In the process of blur kernel estimation, the above approaches will lose some details in the early stage of deblurring for the low-illumination image, Hu *et al.* [29] utilize the light pixels to help low-illumination images deblurring. Roth and Black [30] develop a framework for capturing generic, expressive image statistical priors by extending the traditional Markov random field (MRF) model to learning potential functions over extended pixel neighborhoods.

Recently, sparse regularization and total variation are developed for image deblurring. Xu *et al.* [31] propose a unified framework for both uniform and non-uniform motion deblurring based on the L0 sparse regularization expression. Pan *et al.* [14] utilize the L0-regularized prior on both intensity and gradient to text image deblurring. Xu *et al.* [32] propose an optimization framework by utilizing L0 gradient minimization to generate non-zero gradients, which is resulted in approximate prominent structure in a sparsity-control manner. Chan *et al.* [11], [12], [13] present a type of blind image deblurring algorithm based on the total variation (TV) minimization, which can be regarded as a another image prior. Hintermüller and Rincon-Camacho [33] present a new adapted total variation incorporated with the spatially regularization to reconstruct clear image. Yu *et al.* [34] propose a novel metric able to estimate kernel by measuring the kernel similarity between the neighboring patches of blurred image, and employ the total variation (TV) regularization to estimate the latent image.

The dark channel prior was firstly introduced by He *et al.* [18] for single image dehazing. They utilized to describe the effects of severe weather e.g. haze. Pan *et al.* [19] observe that the dark channel of blurred images is less sparse, compared with clean image. Meanwhile they have proven that optimizing the dark channel helps image restoration and mathematically the observation by using the model of blurred images. Then they utilize the dark channel to generate a dark channel prior for the image deblurring, which can enforce the sparsity of the dark channel and the effect of the image deblurring. Yan *et al.* [20] observe that the bright pixels in the clear images are not likely to be bright after the blur process,

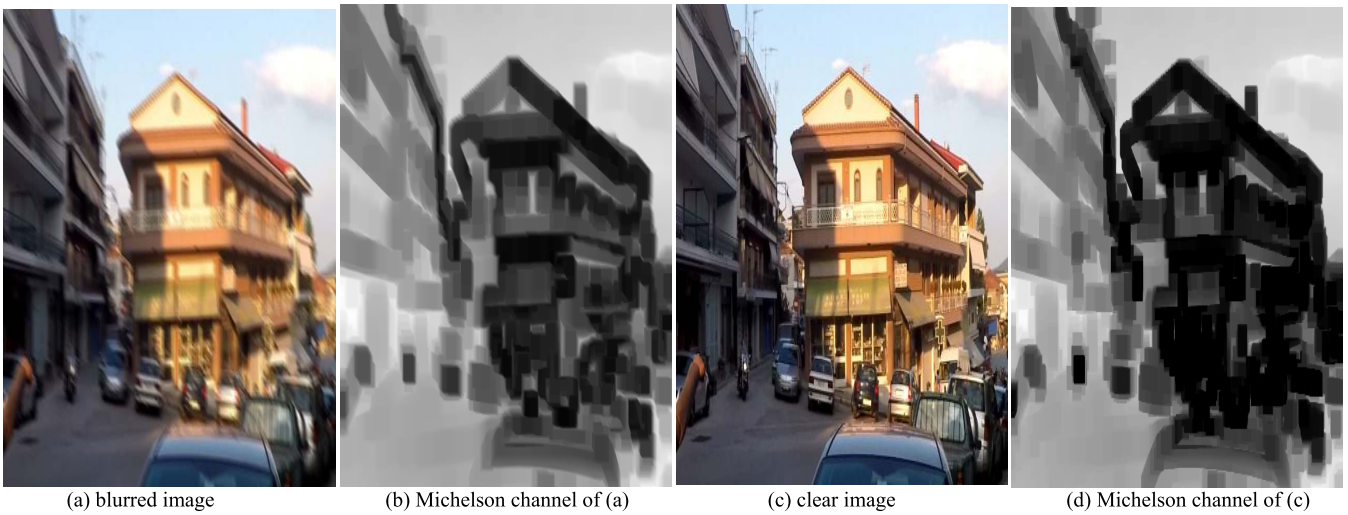

(a) blurred image (b) Michelson channel of (a) (c) clear image (d) Michelson channel of (c)

FIGURE 1. The Michelson channel images of the blurred image and clear image. The Michelson channel pixels of the clear image has a stronger contrast than the Michelson channel of the blurred image. (Best viewed on high-resolution displays with zoom-in).

and then propose a bright channel prior to further leverage the bright and dark information for image deblurring.

III. IMAGE PRIOR AND MICHELSON CHANNLE

In this work, we assume that the noise on the blurred images is small enough to be neglected. According to Eq.(1), the convolution of the discrete blurred image can be defined as the sum of the product of the two signals, which is

$$B(x) = \sum_{z \in \Omega(K)} L(x + \left[\frac{s}{2}\right] - z)K(z) \tag{3}$$

where $\Omega(K)$ and s denote the domain and size of blur kernel, respectively; z denotes the pixels of blur kernel, $K(z) \geq 0$, $\sum_{z \in \Omega(K)} K(z) = 1$ and $[\cdot]$ denotes the rounding operator. With Eq.(3)we can analyze the variation of the image channel of blurred images before and after blurring process.

To explain the role of image patches in image channels clearly, let $\Omega_i(K)$ denote the subsets of $\Omega(K)$ where i denote the number of subsets, we turn the Eq.(3) into the following form,

$$B(x) = \sum_{i} K_i L(x + \left[\frac{s}{2}\right] - i) \tag{4}$$

where $i \in \Omega_i(K)$ and $K_i = K(z)$ i.e. $\sum_i K_i = 1$, $\Omega(k) = \sum_i \Omega_i(k)$.

Note that i denote the i-th image patch, when i is equal to 1, we have $\sum_{z \in \Omega(K)} L(x + \left[\frac{s}{2}\right] - z)K(z) = \sum_i L_i(x + \left[\frac{s}{2}\right] - i)K_i$.

A. MICHELSON CHANNEL PRIOR

In this subsection, a novel statistical prior for image deblurring is presented, i.e., Michelson channel prior (MCP), and then prove this prior mathematically. The proposed prior is based on the observation that the channel of the image has pixels with different intensities at different positions, including weak, strong, etc., wherein the channel with the strongest pixel is called a bright channel, and the channel with the strongest pixel is called a dark channel, but it also includes the middle Color channel. And image channel based on image block creation, different image blocks, with separate blur kernels.

$$M(B)(x) = \frac{\alpha R(B)(x) + (1-\alpha)D(B)(x)}{255 - R(B)(x) + D(B)(x)} \tag{5}$$

where $\alpha (0 \leq \alpha \leq 1)$ denote the adjustment parameter (when $\alpha = 0$, it means the Michelson channel is mainly influenced by dark channel; when $\alpha = 1$, it means the Michelson channel is mainly influenced by bright channel; when $0 < \alpha < 1$, it means the Michelson channel should consider more types of image channel); $D(\cdot)$ and $\mathrm{R}(\cdot)$ denote the dark channel and bright channel operator, respectively; the adjustment parameter, dark channel and bright channel are defined as follows.

$$D(B)(x) = \min_{y \in \Omega(x)} \left(\min_{c \in \{r,g,b\}} B^c(y) \right) \tag{6}$$

$$R(B)(x) = \max_{y \in \Omega(x)} \left(\max_{c \in \{r,g,b\}} B^c(y) \right) \tag{7}$$

where B^c represent the c-th color channel of blurred image. We can observe from Eqs. (5-8), the Michelson channel is the outcome of five operators, containing $\min_{y \in \Omega(x)}$, $\min_{c \in \{r,g,b\}}$, $\max_{y \in \Omega(x)}$, $\max_{c \in \{r,g,b\}}$ and mean$(\cdot)$. If the input image is a gray-scale image, we have $\min_{c \in \{r,g,b\}} B^c(y) = \max_{c \in \{r,g,b\}} B^c(y) = B(y)$.

The results are presented in the Fig. 2, it shows the histogram of the average number of Michelson channel pixels, where the blue and the red histogram denote the Michelson channel of the clear and the blurred image, respectively. As can be observed, we find that clearer image has fewer Michelson channel pixels, comparing with the corresponding

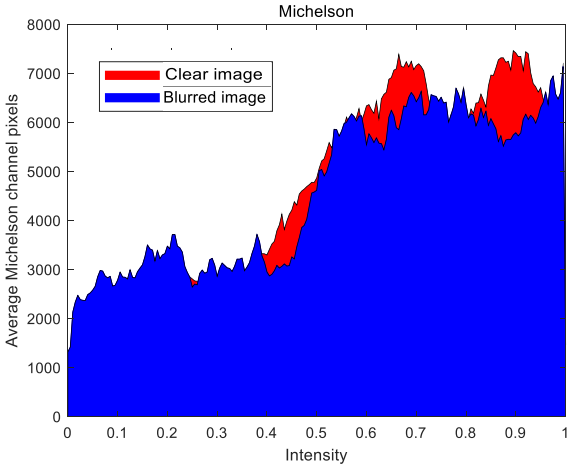

FIGURE 2. Intensity histograms of Michelson channels of both clear and blurred images in various natural images. The results of Michelson channel pixels of images show that clear image has the fewer Michelson channel pixels close to the value between 0.5 and 0.9 comparing with the corresponding blurred image, which is mainly reflected in the green rectangle. The Michelson channel of each image is computed with an image patch size of 35 × 35.

blurred image. Then the Michelson channel is modeled as

$$\begin{aligned} M(B)(x) &= \frac{\alpha \max\limits_{y\in\Omega(x)}(B(y)) + (1-\alpha)\min\limits_{y\in\Omega(x)}(B(y))}{255 - \max\limits_{y\in\Omega(x)}(B(y)) + \min\limits_{y\in\Omega(x)}(B(y))} \\ &= \frac{\alpha\sum_i K_i \max\limits_{y\in\Omega(x)} L_i(y) + (1-\alpha)\sum_i K_i \min\limits_{y\in\Omega(x)} L_i(y)}{255 - \sum_i K_i \max\limits_{y\in\Omega(x)} L_i(y) + \sum_i K_i \min\limits_{y\in\Omega(x)} L_i(y)} \\ &= \sum_i K_i \frac{\alpha \max\limits_{y\in\Omega(x)} L_i(y) + (1-\alpha)\min\limits_{y\in\Omega(x)} L_i(y)}{255 - \max\limits_{y\in\Omega(x)} L_i(y) + \min\limits_{y\in\Omega(x)} L_i(y)} \end{aligned} \tag{8}$$

where $L_i(y) = L\left(y + \left[\frac{s}{2}\right] - i\right)$ and the maximum value of i is equal to the number of image patches $\Omega(x)$, which means that one of the i value corresponds to one of the image patches. Among them, the size format of the image patch is $n \times n$.

According to the Eq.(8), the Michelson channel is formed on a series of image patches $\Omega(x)$ centered at x. However, even if the same deblurring method is applied to estimate the blur kernel of different image patches of an image, the estimated results are different, which is shown in Fig. 3. In order to estimate the integral blur kernel more accurately, we added weights to the blur kernel referred to the corresponding image patches. The equation (9) can be expressed as

$$M(B)(x) = \sum_i \beta_i K_i \frac{\alpha \max\limits_{y\in\Omega(x)} L_i(y) + (1-\alpha)\min\limits_{y\in\Omega(x)} L_i(y)}{255 - \max\limits_{y\in\Omega(x)} L_i(y) + \min\limits_{y\in\Omega(x)} L_i(y)} \tag{9}$$

where β_i denotes the image patches weights at the pixel z of blur kernel.

As shown in Figure 3, the blur kernels in different parts of the figure have a certain difference from the blur kernel of the complete figure. To estimate the latent image more accurately, we need to get a reasonable value of β_i. Inspired by the idea of [34], we propose a new metric algorithm to calculate the corresponding values, the model is as follows.

$$\begin{cases} b = \sum_i sum\left(abs\left(SVD\left(K_i L_i^{dark}\right)\right)\right) \\ c_i = sum\left(abs\left(SVD\left(K_i L_i^{dark}\right)\right)\right) \\ a_i = \prod_i \left(1 - \exp\left(\frac{1}{b} c_i\right)\right) \\ \beta_i = \frac{a_i}{\sum_i a_i} \end{cases} \tag{10}$$

where $sum(\cdot)$, $abs(\cdot)$, and $SVD(\cdot)$ denote the sum, absolute value and matrix singular value operator, respectively; L_i^{dark} denotes the dark channel of the image patch L_i.

To further eliminate the ringing effect caused by image channels as much as possible, we conducted further analysis.

Property 1: blind image deblurring basically requires the recovery of L given the blurred B and the image prior $Pr(B)$, which can be reformulated by obtaining the largest joint probability of (L, K) given B and $Pr(B)$. Based on Bayes' theorem, we further derive.

$$\begin{aligned} P(L, K|B, Pr(B)) &= \frac{P(B, Pr(B)|L, K)\,P(L, K)}{P(B, Pr(B))} \\ &\propto P(B|L, K)\,P(Pr(B)|L, K)\,P(L)\,P(K) \end{aligned} \tag{11}$$

where $P(B|L,K)$ corresponds to the blur process; $P(Pr(B)|L,K)$ represents the relationship between the latent image, blur kernel and the image prior; $P(L)$ and $P(K)$ denote the information of latent image and the blur kernel, respectively.

Property 2: based on the Property 1, the optimal estimation of K and L can be solved by the following optimization problem

$$\begin{aligned} f_{K,L}(K, L) = \arg\min_{K,L} &\|B - L * K\|_2^2 + \varepsilon \|K\|_2^2 + \varsigma \|\nabla L\|_0 \\ &+\xi \|Pr(L)\|^{\rho_1} + \lambda \|\nabla L - \nabla(Pr(L))\|^{\rho_2} \end{aligned} \tag{12}$$

where α, β, ε and λ are weight parameters; $\rho_1, \rho_2 \in [0, 1)$; ∇_h and ∇_v $\left(\nabla = \sum\{\nabla_h, \nabla_v\}\right)$ denote the partial derivative operator in horizontal and vertical directions, respectively.

In the Property 2, $Pr(\cdot)$ is one of main determinant for the deblurring performance, which is referred to the Michelson channel prior.

Property 3: Let $M(\mathrm{B})$ and $M(\mathrm{L})$ denote the Michelson channel of the blurred and clear images, respectively, we have:

$$\begin{aligned} M(B)(x) &= \sum_i \beta_i K_i \frac{\alpha \max\limits_{y\in\Omega(x)} L_i(y) + (1-\alpha)\min\limits_{y\in\Omega(x)} L_i(y)}{255 - \max\limits_{y\in\Omega(x)} L_i(y) + \min\limits_{y\in\Omega(x)} L_i(y)} \\ &\le \sum_i \beta_i K_i \frac{\alpha \max\limits_{y\in\Omega(x)} L(y) + (1-\alpha)\min\limits_{y\in\Omega(x)} L(y)}{255 - \max\limits_{y\in\Omega(x)} L(y) + \min\limits_{y\in\Omega(x)} L(y)} \\ &\le \frac{\alpha \max\limits_{y\in\Omega(x)} L(y) + (1-\alpha)\min\limits_{y\in\Omega(x)} L(y)}{255 - \max\limits_{y\in\Omega(x)} L(y) + \min\limits_{y\in\Omega(x)} L(y)} \sum_i \beta_i K_i \end{aligned}$$

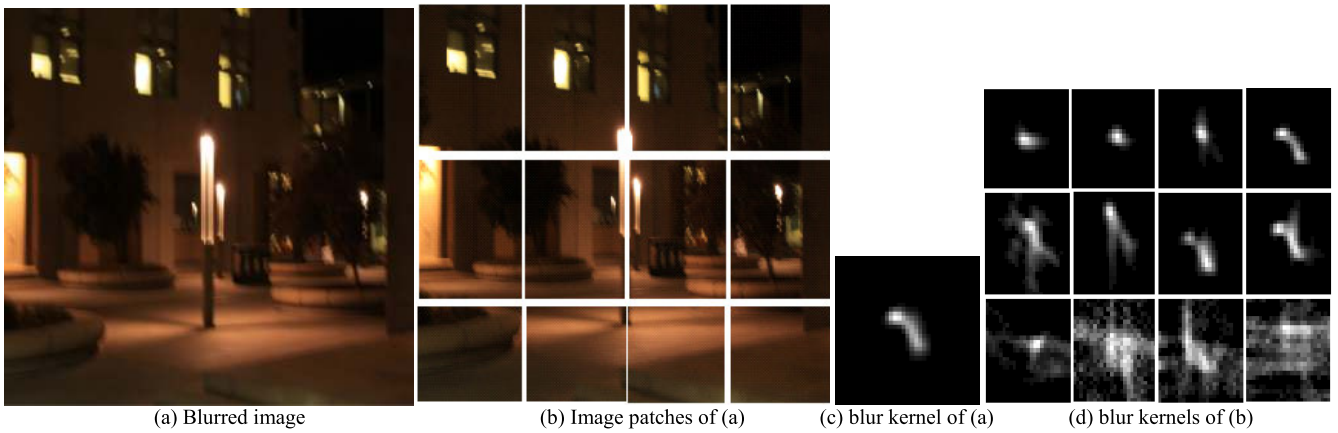

(a) Blurred image (b) Image patches of (a) (c) blur kernel of (a) (d) blur kernels of (b)

FIGURE 3. The blur kernels of image and its patches. The blur kernel is computed with an image patch size of 35 × 35. Wherein subfigure (c) is the blur kernel of subfigure (a); a series of blur kernels in subfigure (d) correspond to each subfigure of the same position in subfigure (d) respectively.

$$= \frac{\alpha \max\limits_{y\in\Omega(x)} L(y) + (1-\alpha) \min\limits_{y\in\Omega(x)} L(y)}{255 - \max\limits_{y\in\Omega(x)} L(y) + \min\limits_{y\in\Omega(x)} L(y)} = M(L)(x) \tag{13}$$

where $\max\limits_{y\in\Omega(x)} L_i(y) \leq \max\limits_{y\in\Omega(x)} L(y)$ and $\min\limits_{y\in\Omega(x)} L_i(y) \geq \min\limits_{y\in\Omega(x)} L(y)$ according the works [19] and [20]; $\sum_i \beta_i K_i = K\mathrm{I}$.

In addition, it is known that $\alpha \max\limits_{y\in\Omega(x)} L(y) \geq 0$ and $(1-\alpha) \min\limits_{y\in\Omega(x)} L(y)$, then according to the (13), we can obtain that

$$M(B)(x) \leq \frac{\alpha R(L)(x)}{255 - R(L)(x) + D(L)(x)} \tag{14}$$

$$M(B)(x) \leq \frac{(1-\alpha) D(L)(x)}{255 - R(L)(x) + D(L)(x)} \tag{15}$$

where $D(L)(x)$ denote the dark channel of clear image. Meanwhile, it means that by adjusting the value of the parameter $\alpha(0 \leq \alpha \leq 1)$, the Michelson channel can takes into consideration of pixel between dark and bright pixels, besides the dark and bright pixels, which are also reflected in the Figure 2 in other side.

Refer to the Eq. (14) demonstrates that the Michelson channel of a blurry image has lower pixels intensities than the corresponding clear image. Therefore, to effectively estimate the blur kernel, another property is introduced, which embodied that the blur process reduces pixels values. Formally, we have

$$\|1 - M(B)(x)\|_0 \geq \|1 - M(L)(x)\|_0 \tag{16}$$

To validate this observation, we have did the statistics experiments in the PASCAL 2012 dataset. Figure 2 show that the value of Michelson channel of the clear images has fewer pixels with the value 0 and 1 comparing the pixels value of the corresponding blurred images. The statistical observation further proves our analysis. Therefore, refer to (13), we add the corresponding L_0-norm sparsity as a regularization term into the process of image deblurring.

B. PROPOSED APPROACH

Based on the above analysis and observation, $\|1 - M(L)(x)\|_0$ norm is applied to measure the sparsity of the Michelson channels, corresponding to the $Pr(\cdot)$ in Property 2. According to the Property 2 and Property 3, we present the blind image deblurring model and develop an efficient optimization method for the kernel and the latent image estimation, by measuring and adjusting the of image channel sparsity of the blurred image. The presented blind deblurring method can be formulated as

$$f_{K,L}(K,L) = \arg\min_{K,L} \|B - L*K\|_2^2 + \varepsilon \|K\|_2^2 + \varsigma \|\nabla L\|_0 + \xi \|1 - M(L)\|_0 + \lambda \|\nabla L - \nabla(M(L))\|_0 \tag{17}$$

where the first term of Problem (17) is used to guarantee the accuracy of the deblurring image and the estimated blur kernel is similar to the truly blur kernel; the second term is applied to control the solution of the blur kernel by using the L_2 norms; the third term is employed to make the estimated image smoothing; the fourth term is applied to enhance the Michelson channel pixels of latent image; the final term of the formula is used to decrease the ringing artifacts caused by the Michelson channel prior; ζ, ξ, ε and λ are weight parameter.

1) INTERMEDIATE LATENT IMAGE ESTIMATION

To estimate the final latent image (clear image), the algorithm alternatively update the intermediate blur kernel and latent image. In the alternatively deconvolution steps, in order to estimate the latent image L, an initial blur kernel K should be given. Then by using the input blurred image B, we use an energy function to obtain the intermediate image according to the equation (9), which is summarized as

$$\min_L \|B - L*K\|_2^2 + \varsigma \|\nabla L\|_0 + \xi \|1 - M(L)\|_0 + \lambda \|\nabla L - \nabla M(L)\|_0 \tag{18}$$

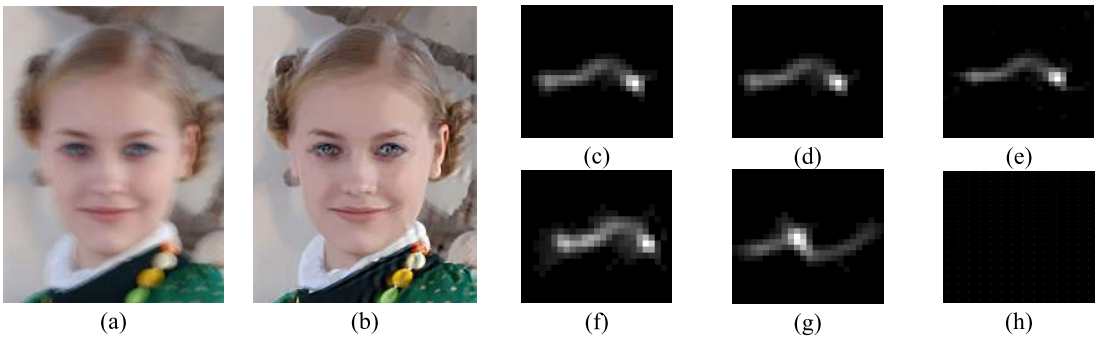

FIGURE 4. kernel estimation(a: blurred image; b: our deblurred image; Fig.4(c-h) denote the kernel estimation of ours, Liu *et al.* [12], Xu and Jia *et al.* [9], Jia [25], Lai *et al.* [4] and Liu *et al.* [13], respectively).

where $\nabla L \in \{\nabla_h L, \nabla_v L\}$ corresponding to the gradients of the intermediate latent image; $\nabla M(L) \in \{\nabla_h M(L), \nabla_v M(L)\}$ corresponding to the gradients of Michelson channel of the intermediate latent image.

Because the L_0-regularized term of the Michelson channel and its gradients are computationally intractable in image deblurring, half-quadratic splitting L_0 minimization approach [32] is employed to optimize the problem (10) with respect to intermediate latent image, which is

$$\begin{aligned}\left\{\hat{L}, \hat{g}, \hat{\mu}, \hat{\nu}\right\} = \arg\min_{L,g,\mu,\nu} \|B - L * K\|_2^2 + \gamma \|\nabla L - g\|_2^2 \\ +\eta \|1 - M(L) - p\|_2^2 + \kappa \|\nabla L - \nabla M(L) \\ -q\|_2^2 + \varsigma \|g\|_0 + \xi \|p\|_0 + \lambda \|q\|_0 \end{aligned} \tag{19}$$

where λ, η and κ denote penalty parameters; g, p and q denote the optimization variable corresponding to the ∇L , $1-M(L)$ and $\nabla L - \nabla M(L)$; $g = (g_h, g_v)$ and $q = (q_h, q_v)$ denote the image gradients in the horizontal and vertical directions.

When the value of parameters γ, η and κ can be determined and reasonable, the solution of (19) can be solved by alternatively update, that is, the optimization of L, g, p and q can be minimized by fixed other variables, which will be represented in our work.

To estimate the latent image L, the optimization function will become as

$$\begin{aligned}\hat{L} = \min_{L} \|B - L * K\|_2^2 + \gamma \|\nabla L - g\|_2^2 \\ +\eta \|1 - M(L) - p\|_2^2 + \kappa \|\nabla L - \nabla M(L) - q\|_2^2 \end{aligned} \tag{20}$$

In the Problem (19), the non-linear operation M(L) is equivalent to a linear operator M, which is applied to represent the vector matrix of the dark channel D(L),

$$F(x, y) = \begin{cases} 1, & y = \min\limits_{y \in \Omega(x)} L(y); \\ 0, & otherwise. \end{cases} \tag{21}$$

During the deblurring process, F is applied to estimate the intermediate latent image. When the intermediate image approaches the clear image, the computed is similar to the dark channel operation $D(\cdot)$. Given the intermediate latent image L, the mapping matrices F_L and F_{1-L} denote to $D(L)$ and $255-R(L)$, respectively. Then, the objective function yield as

$$\begin{aligned}\hat{L} = \min_{L} \|B - L * K\|_2^2 + \gamma \|\nabla L - g\|_2^2 \\ +\eta \left\| 1 - \frac{F_{1-L} - F_L}{255 - F_{1-L} + F_L} - p \right\|_2^2 \\ +\kappa \left\| \nabla L - \nabla \left(\frac{F_{1-L} - F_L}{255 - F_{1-L} + F_L} \right) - q \right\|_2^2 \end{aligned} \tag{22}$$

Then for the formulation of latent image estimation Problem (21), we use the matrix-vector form to optimize and solve it, which is formulated as

$$\begin{aligned}\hat{\boldsymbol{L}} = \min_{\mathbf{L}} \|\mathbf{B} - \mathbf{L}\mathbf{K}\|_2^2 + \gamma \|\nabla \mathbf{L} - \mathbf{g}\|_2^2 \\ +\eta \left\| 1 - \frac{\mathbf{F}_{1-L} - \mathbf{F}_L}{255 - \mathbf{F}_{1-L} + \mathbf{F}_L} - \boldsymbol{p} \right\|_2^2 \\ +\kappa \left\| \nabla \mathbf{L} - \nabla \left(\frac{\mathbf{F}_{1-L} - \mathbf{F}_L}{255 - \mathbf{F}_{1-L} + \mathbf{F}_L} \right) - \boldsymbol{q} \right\|_2^2 \end{aligned} \tag{23}$$

where $\mathbf{B}$ is the matrix form of B with respect to blur kernel $\mathbf{K}$; $\mathbf{F}$, $\mathbf{K}$, $\mathbf{g}$, $\mathbf{p}$ and $\mathbf{q}$ denote the matrix form of F, K, g, p and q, respectively.

For the latent image $\mathbf{L}$, it can be solved efficiently using the FFT and its inverse based on the Problems (22) and (23), which the closed-form solution yield as

Where $\Phi(\cdot)$ and $\Phi^{-1}(\cdot)$ denote the denote the Fast Fourier transform and its inverse transform, respectively; $\overline{\mathcal{F}(\cdot)}$ represent the complex conjugate operator; and in which $\boldsymbol{F}_K = \overline{\mathcal{F}(K)}\mathcal{F}(K)$, $\boldsymbol{F}_g = \overline{\mathcal{F}(\nabla L_h)}\mathcal{F}(g_h) + \overline{\mathcal{F}(\nabla L_v)}\mathcal{F}(g_v)$, $\boldsymbol{F}_p = \overline{\mathcal{F}(p)}\mathcal{F}(p)$; $\boldsymbol{F}_q = \overline{\mathcal{F}\left(\nabla L_h - \nabla M(L)_h\right)}\mathcal{F}\left(\nabla L_h - \nabla M(L)_h\right) + \overline{\mathcal{F}\left(\nabla L_v - \nabla M(L)_v\right)}\mathcal{F}\left(\nabla L_v - \nabla M(L)_v\right)$.

Given the intermediate latent image, the sub-problems with respect to g, p and q can be solved separately by:

$$\hat{g} = \min_{g} \gamma \|\nabla L - g\|_2^2 + \varsigma \|g\|_0 \tag{25}$$

$$\hat{p} = \min_{p} \eta \|M(L) - p\|_2^2 + \xi \|p\|_0 \tag{26}$$

$$\hat{q} = \min_{\nu} \kappa \|\nabla L - \nabla M(L) - q\|_2^2 + \lambda \|q\|_0 \tag{27}$$

According to work [19], [31], Problem(20) is a pixel-wise minimization problem, thus the solution of q and p can be

$$L = \mathcal{F}^{-1}\left(\frac{\overline{\mathcal{F}(K)}\mathcal{F}(B) + \gamma \boldsymbol{F}_g + \eta \boldsymbol{F}_p + \kappa \boldsymbol{F}_q}{\boldsymbol{F}_K + \gamma\left(\overline{\mathcal{F}(\nabla L)}\mathcal{F}(\nabla L)\right) + \eta + \kappa\left(\overline{\mathcal{F}\left(\nabla L - \nabla M(L)\right)}\mathcal{F}\left(\nabla L - \nabla M(L)\right)\right)}\right) \tag{24}$$

obtained by:

$$p = \begin{cases} M(L), & \|M(L)\|_2^2 \geq \dfrac{\xi}{\eta} \\ 0, & otherwise \end{cases} \tag{28}$$

$$q = \begin{cases} \nabla L - \nabla M(L), & \|\nabla L - \nabla M(L)\|_2^2 \geq \dfrac{\lambda}{\kappa} \\ 0, & otherwise \end{cases} \tag{29}$$

The specific step of our method for intermediate latent image and blur kernel estimation is summarized in Algorithm 1.

2) INTERMEDIATE BLUR KERNEL ESTIMATION

In the step of intermediate latent image estimation in Algorithm 1, the blur kernel should be updated. The optimization along with K can be directly extended to handle motion deblurring by given intermediate L. Based on the Problem(6), the optimization can be formulated as

$$\min_K \ \|\nabla B - \nabla L * K\|_2^2 + \varepsilon \|K\|_2^2 \tag{30}$$

For simplicity, the matrix-vector form of non-uniform blur process (Problem(7)) can be expressed as

$$\min_{\mathbf{K}} \ \|\nabla \mathbf{B} - \nabla \mathbf{L} * \mathbf{K}\|_2^2 + \varepsilon \|\mathbf{K}\|_2^2 \tag{31}$$

Obviously, it is a least squares minimization problem, which is similar to the existing approaches [32], [35]. By using the FFT and given an intermediate latent image,

Algorithm 1 Solving (17)

Input: blur image B;
initialize blur kernel K
$L \leftarrow B$, $\varsigma \leftarrow 2\gamma$, $\xi \leftarrow 2\eta$, $\lambda \leftarrow 2\kappa$
while i≤max_iter **do**
repeat
solve g for using Problem (25)
repeat
solve p for using Problem (26)
repeat
solve q for using Problem (27)
solve L for using Problem (24)
until
until
until
solve K for using Problem (32)
end while
Output: intermediate latent image L and blur kernel K

the solution of blur kernel K is yield as

$$\hat{K} = \mathcal{F}^{-1}\left(\frac{\overline{\mathcal{F}(\nabla L)}\mathcal{F}(\nabla B)}{\overline{\mathcal{F}(\nabla L)}\mathcal{F}(\nabla L) + \varepsilon}\right) \tag{32}$$

When the K are obtained, the negative elements of K are set to 0, and then normalize K. meanwhile, similar to other deblurring methods [19], the proposed blur kernel estimation process is carried out by using an image pyramid [36] with a coarse-to-fine manner.

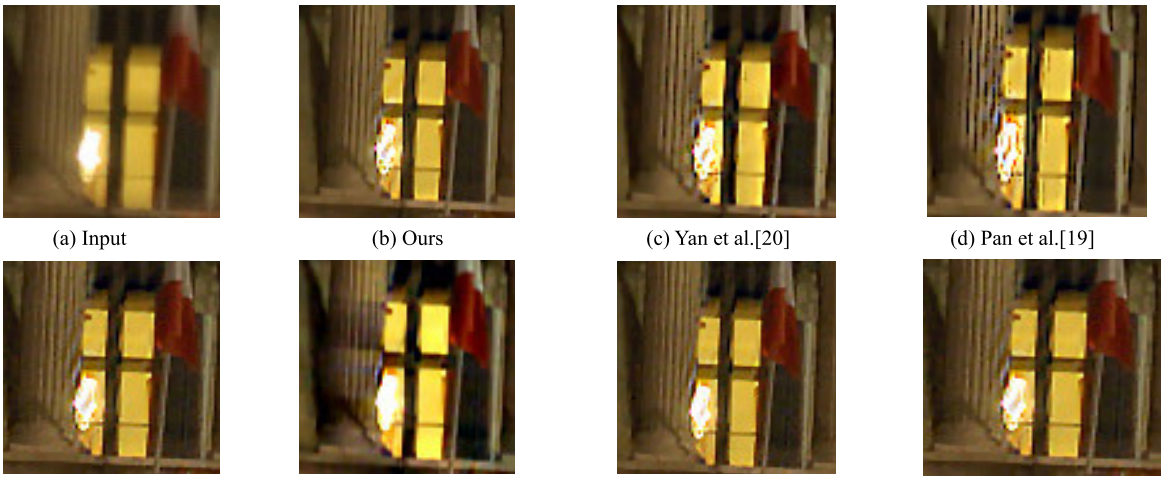

(a) Input (b) Ours (c) Yan et al.[20] (d) Pan et al.[19]
(e) Cho et al.[36] (f) Pan et al.[14] (g) Xu et al. [9] (e) Krishnan et al.[38]

FIGURE 5. Comparison of a low-illumination image deblurring. The deblurring results are generated by various non-blind deblurring methods. The blur kernel estimations exist in the bottom right corner of sub-image (Best viewed on high-resolution display with zoom-in.).

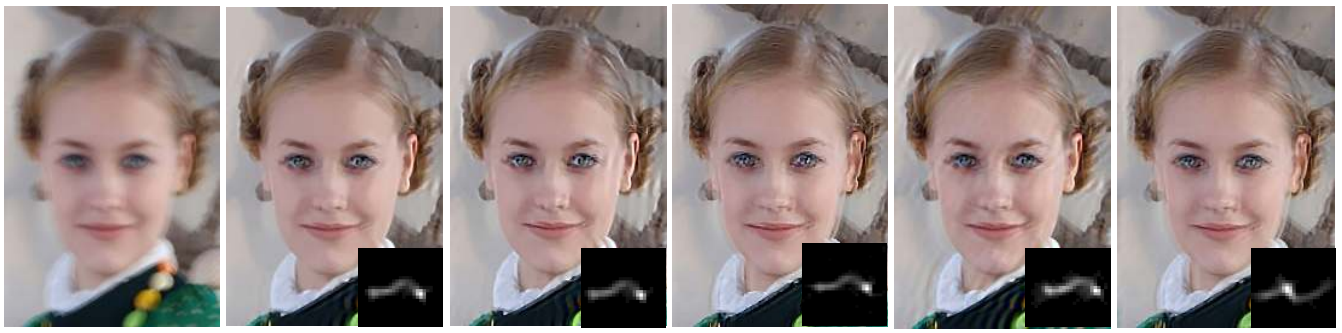

(a)Input (b) Ours (c) Yan et al.[20] (d) Levin et al.[16] (e) Pan et al.[19] (f) Xu et al. [9]

FIGURE 6. Comparison of face image deblurring. Our method compares favorably with [9], [16], [19], [20], which generating less ringing artifacts. And other methods apply typical image prior or explore the face features for the face image deblurring (Best viewed on high resolution display with zoom-in.).

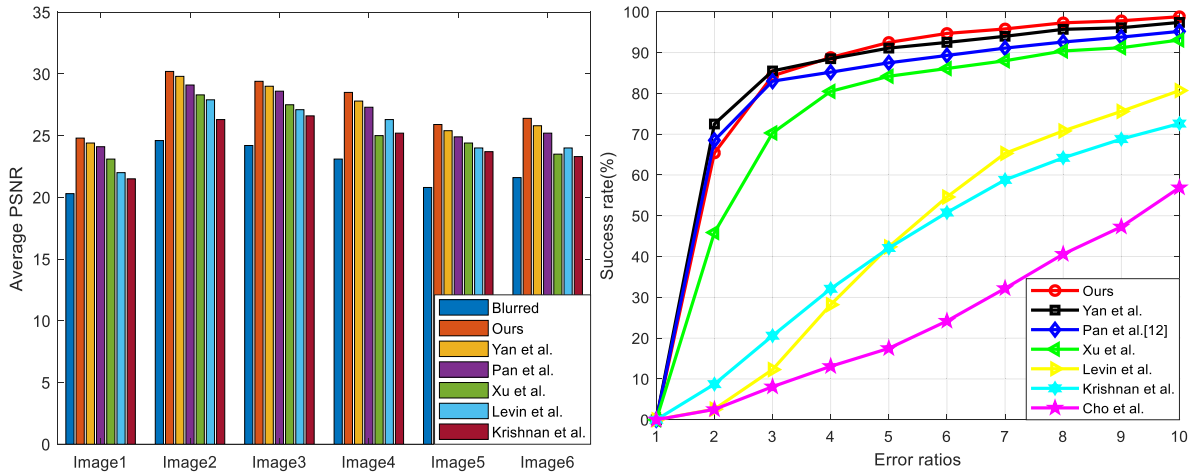

(a) Results of PSNR[40] (b) Results of Success rate[41]

FIGURE 7. Quantitative evaluations of PSNR and Success rate on the two benchmark datasets. Our method performs competitively against the state-of-the-art.

After determining the weights, we alternatively estimate the intermediate latent image and blur kernel. The specific optimization algorithms with respect to the blur kernel and latent image are represented in Section 3. The main steps of the proposed method are shown in the Algorithm 1.

IV. EXPERIMENTS

In this section, we will represent the deblurring performance of our proposed method on both the synthetic and real images, and then compare its performance with other deblurring methods. In all experiments, some parameters are set as follows: $\varsigma = \xi = \lambda = 0.004$, $\varepsilon = 2$; the maximum iteration of proposed method max iteration: max_iter $= 5$; the dark channel of each image is computed by an image patch size of 35×35.

A. DEBLURRING THE NATURAL IMAGES

To show the deblurring performance of our method, firstly, we test its deblurring performance on the two natural image deblurring datasets from the work [10], [19]; secondly, we compare our method with other state-of-the-art deblurring methods [9], [10], [16], [19], [37]. In the natural word, there exists many types of blurred images, and we mainly evaluate and compare the deblurring performances of various methods on the typical blurred images, including the text image [14], face image [19], and low-illumination image [10]. The some deblurring results on different blurred images have been represented in the experiment.

1) LOW-ILLUMINATION MOTION BLURRED IMAGE

low-illumination blurred images are not conducive to image restoration due to the influence for the kernel estimation [19], [29]. Especially, compared with the clean image, the blurred images have the less Michelson channel pixels. And the dark channel prior [19] and bright channel prior [20] are applied to mainly extract the dark channel and bright channel pixel of blurred images, respectively. However, our method can estimate the image blur kernel more clearly and efficiently by using the information of the Michelson channel, the results have been shown in Fig. 5.

2) TEXT MOTION BLURRED IMAGE

In the semantic clues of character recognition and image understanding, the deblurring of blurred text image can help

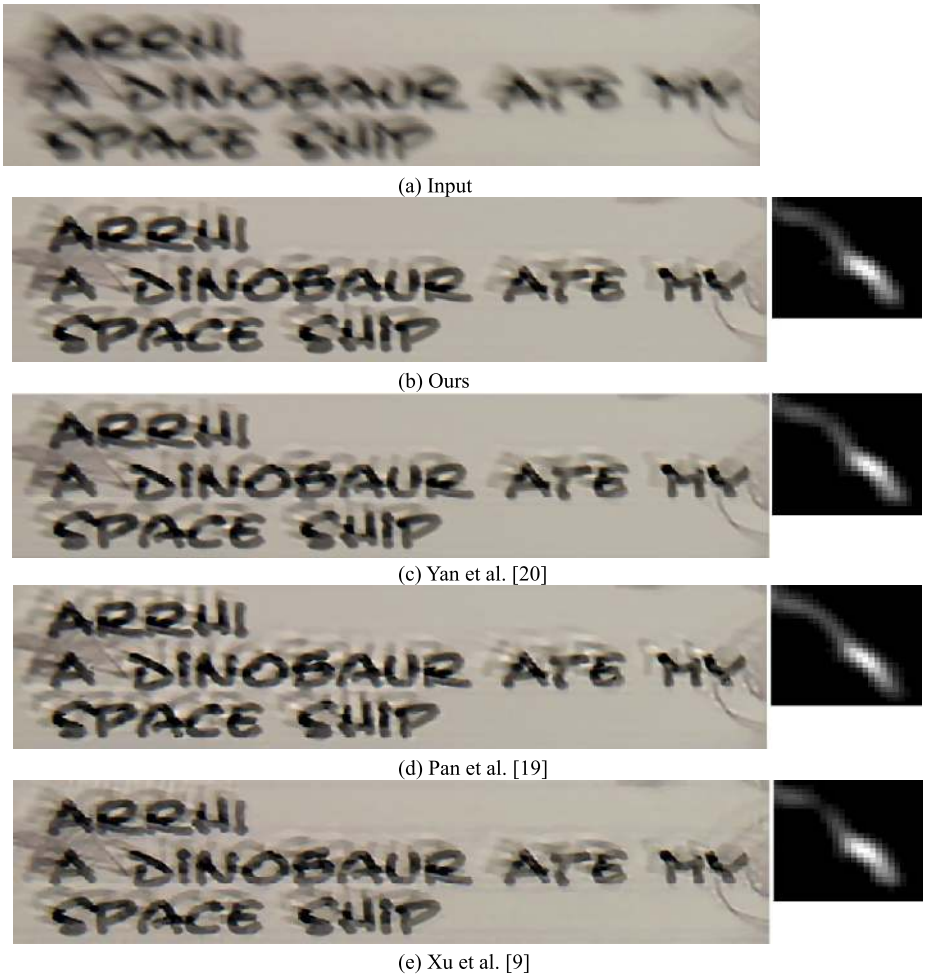

FIGURE 8. Comparison of text images deblurring; our method generates result comparable to the results of the Yan *et al.* [20], and better than the method tailored to text, e.g. the works [9], [19] (Best viewed on high resolution display with zoom-in.).

to further understand the real world [14]. Simultaneously, in the text image deblurring, we need to focus on the characters, which will make the deblurring process be more difficult, the results are shown in Fig. 6.

3) FACE MOTION BLURRED IMAGES

Due to the texture structure of the face, it has fewer edges or characteristics, which will bring certain challenges to the blur kernel estimation in the image restoration process, and finally make the negative effect for the face image deblurring. As shown in Fig. 7, our method contain better deblurring performance in the face image deblurring, compared with the [[9], [19], [20] etc.]

In [19], dark channel prior has been proved that it can help generate the better blur kernel and latent image estimation on the various types of blurred images. According to the dark channel prior, Yan et al. present a bright channel prior for image deblurring. Our experiments on Michelson channel prior further carry out the deblurring experiments (As shown in Figs. 5, 6 and 7) on the building, text and face blurred images to demonstrate the effectiveness of our method.

Compared with other methods, it visually shows our method obtains the better or equivalent deblurring performance on the three challenging blurred image. In summary, our deblurring method can produce less ringing artifacts compared with deblurring images generated by other methods [[9], [16], [19], [20] etc.] and generate the significant image channel pixels.

B. QUANTITATIVE EVALUATION

To further obtain the performance of existing deblurring method, we adopt an Image Quality Assessment (IQA): Peak Signal to Noise Ratio (PSNR) and the success rate between the clear image and deblurring image to evaluate the performance compared with other methods. We choose some blurred image from the image dataset given by Google (GPORO) and the image dataset by Köhler *et al.* [40]. The PSNR value is calculated by comparing the recovered image with ground truth images captured.

From the Fig. 8, compared with the method in [[9], [16], [19], [20], [35] etc.], our method obtain the higher PSNR value and the better Success Rate curve. Meanwhile, the

deblurring method by using image channel prior containing ours, Yan et al. and Pan et al. obtain better deblurring performance, which further demonstrate the effectiveness of the image channel in the blind image deblurring. But still, our method's performance is better.

As shown in Figs. 5–7, it directly demonstrates that the reasonable use of the information of the Michelson channel can further eliminate the ringing effect of the image and enhance the image channel pixels of the restored image. It is helpful for blur kernel estimation and latent image estimation for the various typical image deblurring. In summary, appropriate application of the Michelson channel of the image and its gradient information can generate the better clear image.

V. CONCLUSION

Appropriate use of dark channel and bright channel in the blurred image can help improve the results of blind image deblurring, but certain ringing artifacts will also be added in the deblurring process. In this paper, we noticed the difference between the series of image patches of natural images and found that the image pixels of blurred images will decrease after blurring process. Based on this observation a new deblurring image channel prior for image deblurring is proposed, which is called Michelson channel. Meanwhile, by appropriately use the channel information of the corresponding image patches, our method can help further capture the Michelson channel pixels of sharp image, remove the ringing artifacts, and make the Michelson channel pixels of deblurring image more stable. The proposed deblurring framework takes both the Michelson channel and its image patches' information into consideration, and does not require any complex pre-process step (edge detection or selection e.g.). Massive experimental results show that our method outperforms multiple existing deblurring methods on both the synthesized and natural images.

REFERENCES

[1] D. Gong, M. Tan, Y. Zhang, A. van den Hengel, and Q. Shi, "Self-paced kernel estimation for robust blind image deblurring," in *Proc. IEEE Int. Conf. Comput. Vis. (ICCV)*, Oct. 2017, pp. 1670–1679.

[2] S. K. Nayar and M. Ben-Ezra, "Motion-based motion deblurring," *IEEE Trans. Pattern Anal. Mach. Intell.*, vol. 26, no. 6, pp. 689–698, Jun. 2004.

[3] D. Gong, M. Tan, Q. Shi, A. van den Hengel, and Y. Zhang, "MPTV: Matching pursuit-based total variation minimization for image deconvolution," *IEEE Trans. Image Process.*, vol. 28, no. 4, pp. 1851–1865, Apr. 2019.

[4] W.-S. Lai, J.-B. Huang, Z. Hu, N. Ahuja, and M.-H. Yang, "A comparative study for single image blind deblurring," in *Proc. IEEE Conf. Comput. Vis. Pattern Recognit.*, Jun. 2016, pp. 1701–1709.

[5] J. Liu, W. Yang, X. Zhang, and Z. Guo, "Retrieval compensated group structured sparsity for image super-resolution," *IEEE Trans. Multimedia*, vol. 19, no. 2, pp. 302–316, Feb. 2017.

[6] C. Min, G. Wen, B. Li, and F. Fan, "Blind deblurring via a novel recursive deep CNN improved by wavelet transform," *IEEE Access*, vol. 6, pp. 69242–69252, 2018.

[7] M. Donatelli and M. Hanke, "Fast nonstationary preconditioned iterative methods for ill-posed problems, with application to image deblurring," *Inverse Problems*, vol. 29, no. 9, 2013, Art. no. 095008.

[8] J. M. Bardsley and A. Luttman, "Total variation-penalized Poisson likelihood estimation for ill-posed problems," *Adv. Comput. Math.*, vol. 31, nos. 1–3, pp. 35–59, 2009.

[9] L. Xu and J. Jia, "Two-phase kernel estimation for robust motion deblurring," in *Proc. Eur. Conf. Comput. Vis.* Berlin, Germany: Springer, 2010.

[10] J. Pan, R. Liu, Z. Su, and X. Gu, "Kernel estimation from salient structure for robust motion deblurring," *Signal Process. Image Commun.*, vol. 28, no. 9, pp. 1156–1170, 2013.

[11] S. T. F. Chan and C.-K. Wong, "Total variation blind deconvolution," *IEEE Trans. Image Process.*, vol. 7, no. 3, pp. 370–375, Mar. 1998.

[12] H. Liu, R. Xiong, X. Zhang, Y. Zhang, S. Ma, and W. Gao, "Nonlocal gradient sparsity regularization for image restoration," *IEEE Trans. Circuits Syst. Video Technol.*, vol. 27, no. 6, pp. 1909–1921, Sep. 2016.

[13] Q. Liu, S. Wang, L. Ying, X. Peng, Y. Zhu, and D. Liang, "Adaptive dictionary learning in sparse gradient domain for image recovery," *IEEE Trans. Image Process.*, vol. 22, no. 12, pp. 4652–4663, Dec. 2013.

[14] J. Pan, Z. Hu, Z. Su, and M.-H. Yang, "Deblurring text images via L0-regularized intensity and gradient prior," in *Proc. IEEE Conf. Comput. Vis. Pattern Recognit.*, Jun. 2014, pp. 2901–2908.

[15] W. Ren, X. Cao, J. Pan, X. Guo, W. Zuo, and M.-H. Yang, "Image deblurring via enhanced low-rank prior," *IEEE Trans. Image Process.*, vol. 25, no. 7, pp. 3426–3437, Jul. 2016.

[16] A. Levin, Y. Weiss, F. Durand, and W. T. Freeman, "Efficient marginal likelihood optimization in blind deconvolution," in *Proc. CVPR*, Jun. 2011, pp. 2657–2664.

[17] N. Joshi, R. Szeliski, and D. J. Kriegman, "PSF estimation using sharp edge prediction," in *Proc. IEEE Conf. Comput. Vis. Pattern Recognit.*, Jun. 2008, pp. 1–8.

[18] K. He, J. Sun, and X. Tang, "Single image haze removal using dark channel prior," in *Proc. IEEE Conf. Comput. Vis. Pattern Recognit.*, Jun. 2009, pp. 1956–1963.

[19] J. Pan, D. Sun, H. Pfister, and M.-H. Yang, "Blind Image Deblurring Using Dark Channel Prior," in *Proc. IEEE Conf. Comput. Vis. Pattern Recognit. (CVPR)*, Jun. 2016, pp. 1628–1636.

[20] Y. Yan, W. Ren, Y. Guo, R. Wang, and X. Cao, "Image deblurring via extreme channels prior," in *Proc. IEEE Conf. Comput. Vis. Pattern Recognit.*, Jul. 2017, pp. 4003–4011.

[21] L. Schaul, C. Fredembach, and S. Süsstrunk, "Color image dehazing using the near-infrared," in *Proc. IEEE Int. Conf. Image Process.*, Nov. 2010, pp. 1629–1632.

[22] J.-H. Kim, W.-D. Jang, J.-Y. Sim, and C.-S. Kim, "Optimized contrast enhancement for real-time image and video dehazing," *J. Vis. Commun. Image Represent.*, vol. 24, no. 3, pp. 410–425, Apr. 2013.

[23] M. Yang, J. Liu, and Z. Li, "Superpixel-based single nighttime image haze removal," *IEEE Trans. Multimedia*, vol. 20, no. 11, pp. 3008–3018, Nov. 2018.

[24] J. Xie, R. S. Feris, and M.-T. Sun, "Edge-guided single depth image super resolution," *IEEE Trans. Image Process.*, vol. 25, no. 1, pp. 428–438, Jan. 2016.

[25] J. Jia, "Single image motion deblurring using transparency," in *Proc. IEEE Conf. Comput. Vis. Pattern Recognit.*, Jun. 2007, pp. 1–8.

[26] Q. Shan, J. Jia, and A. Agarwala, "High-quality motion deblurring from a single image," *Acm Trans. Graph.*, vol. 27, no. 3, pp. 1–10, 2008.

[27] H. Ji and K. Wang, "A two-stage approach to blind spatially-varying motion deblurring," in *Proc. IEEE Conf. Comput. Vis. Pattern Recognit.*, Jun. 2012, pp. 73–80.

[28] A. Rav-Acha and S. Peleg, "Two motion-blurred images are better than one," *Pattern Recognit. Lett.*, vol. 26, no. 3, pp. 311–317, 2005.

[29] Z. Hu, S. Cho, J. Wang, and M.-H. Yang, "Deblurring low-light images with light streaks," in *Proc. IEEE Conf. Comput. Vis. Pattern Recognit.*, Jun. 2014, pp. 3382–3389.

[30] S. Roth and M. J. Black, "Fields of experts: A framework for learning image priors," in *Proc. IEEE Comput. Soc. Conf. Comput. Vis. Pattern Recognit.*, Jun. 2005, pp. 860–867.

[31] L. Xu, S. Zheng, and J. Jia, "Unnatural L0 Sparse Representation for Natural Image Deblurring," in *Proc. IEEE Conf. Comput. Vis. Pattern Recognit.*, Jun. 2013, pp. 1107–1114.

[32] L. Xu, C. Lu, Y. Xu, and J. Jia, "Image smoothing via L0 gradient minimization," *ACM Trans. Graph.*, vol. 30, no. 6, pp. 1–12, 2011.

[33] M. Hintermüller and M. M. Rincon-Camacho, "Expected absolute value estimators for a spatially adapted regularization parameter choice rule in L1-TV-based image restoration," *Inverse Problems*, vol. 26, no. 8, 2010, Art. no. 085005.

[34] X. Yu, F. Xu, S. Zhang, and L. Zhang, "Efficient patch-wise non-uniform deblurring for a single image," *IEEE Trans. Multimedia*, vol. 16, no. 6, pp. 1510–1524, Oct. 2014.

[35] S. Cho and S. Lee, "Fast motion deblurring," *ACM Trans. Graph.*, vol. 28, p. 145, Dec. 2009.
[36] J.-J. Ding, W.-D. Chang, Y. Chen, S.-W. Fu, C.-W. Chang, and C.-C. Chang, "Image deblurring using a pyramid-based Richardson-Lucy algorithm," in *Proc. 19th Int. Conf. Digit. Signal Process.*, Aug. 2014, pp. 204–209.
[37] D. Krishnan, T. Tay, and R. Fergus, "Blind deconvolution using a normalized sparsity measure," in *Proc. CVPR*, Jun. 2011, pp. 233–240.
[38] M. Hirsch, B. Mohler, and S. Harmeling, *Recording and Playback of Camera Shake: Benchmarking Blind Deconvolution with a Real-World Database*, 2012.
[39] L. Sun, S. Cho, J. Wang, and J. Hays, "Edge-based blur kernel estimation using patch priors," in *Proc. IEEE Int. Conf. Comput. Photography*, Apr. 2013, pp. 1–8.
[40] R. Köhler, M. Hirsch, and B. Mohler, *Recording and Playback of Camera Shake: Benchmarking Blind Deconvolution with a Real-World Database*, 2012.

GUOQUAN WEN was born in Yibin, Sichuan, China, in 1994. He received the bachelor's and master's degrees from Southwest Petroleum University, in 2012 and 2019, respectively, where he is currently pursuing the degree. He has published two articles in total. His research interests are image processing and data mining.

CHAO MIN was born in Xindu, Chengdu, China, in 1982. He received the M.S. degree in pure mathematics and the Ph.D. degree in operations and control theory from Sichuan University, Chengdu, in 2007 and 2013, respectively. He is an Associate Professor with the School of Sciences, Southwest Petroleum University, China. His research interests include uncertainty theory and its application, especially in petroleum engineering and image processing. He was a recipient of the Scientific and Technological Progress Award (1st Class) of China National Association for Automation in Petroleum and Chemical Industry (CNPCI), in 2015, and the Scientific and Technological Progress Award (1st Class) of Ministry of Education of PRC, in 2015.

ZEYUN JIANG was born in Chengdu, China, in 1965. He received the M.S. degrees from Sichuan University, in 2007, and the Ph.D. degree from Heriot-Watt University, Edinburgh, U.K., in 2008. Since 2004, he has been mainly engaged in heterogeneous multiscale structural analysis and fluid seepage model research on porous media (such as rock, soil, etc.). He has published more than 40 articles in journals and international conferences, such as *Water Resources Research*, *Transport in Porous Media*, and *Fuel*. He is also mainly engaged in the study of microscopic void structure analysis and network seepage model, the independent development software system PAT – Pore Analysis Tools (this software is widely used in academic and industrial circles), is good at analyzing the geometric topological properties of rock microscopic images.

ZHAOZHONG YANG was born in Luzhou, Sichuan, China, in 1969. He received the M.S. and Ph.D. degrees in oil and gas field development engineering from Southwest Petroleum University, Chengdu, in 1993 and 1996, respectively. He is currently a Professor with the School of Oil and Gas Engineering. His research interests mainly include oil and gas reservoir stimulation mechanical and the related artificial intelligence technology. He is currently an Academic and Technical Leader in Sichuan Province.

XIAOGANG LI was born in Renshou, Sichuan, China, in 1981. He received the M.S. and Ph.D. degrees in oil and gas field development engineering from Southwest Petroleum University, Chengdu, in 2006 and 2009, respectively. He is currently a Professor with the School of Oil and Gas Engineering. His research interests mainly include oil and gas reservoir stimulation mechanical and the related artificial intelligence technology. He was a recipient of the Science and Technology Progress Award (Second Class) of the China National Association for Automation in Petroleum and Chemical Industry, in 2016.